analytical chemistry

Article

Cite This: *Anal. Chem.* 2018, 90, 8337−8344

pubs.acs.org/ac

Internal Calibration Potentiometric Aptasensors for Simultaneous Detection of Hg^{2+}, Cd^{2+}, and As^{3+} Based on a Screen-Printed Carbon Electrodes Array

Wanxin Tang, Zhenzhen Wang, Juan Yu, Fan Zhang,* and Pingang He

School of Chemistry and Molecular Engineering, East China Normal University, 500 Dongchuan Road, Shanghai 200241, P. R. China

Supporting Information

ABSTRACT: An all-solid-state potentiometric aptasensor array based on a multichannel disposable screen-printed carbon electrode (SPCE) was demonstrated for the simultaneous detection of Hg^{2+}, Cd^{2+}, and As^{3+} by open circuit potential (OCP) technology. The potential of the channel with an internal calibration DNA sequence (IC-DNA) was employed as the internal calibration potential (ICP) to subtract the background signal generated by the detection system, providing a built-in correction methodology. As a result, the developed aptasensor array showed high sensitivity and accuracy for detecting Hg^{2+}, Cd^{2+}, and As^{3+} without mutual interference or interference from other ions. The linear response ranged from 2.5 pM to 2.5 μM, and the detection limits for Hg^{2+}, Cd^{2+}, and As^{3+} were 2.0, 0.62, and 0.17 pM, respectively. Furthermore, the potentiometric aptasensor array was successfully applied for the simultaneous detection of three ions in real samples. The results obtained from the developed approach agreed well with the results obtained from inductively coupled plasma mass spectrometry.

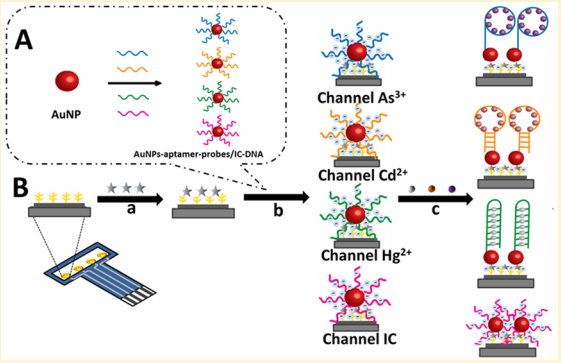

Currently, environmental pollution involving toxic metal ions, especially Hg^{2+}, Cd^{2+}, and As^{3+}, has become an increasingly serious issue, and it poses a severe threat to ecosystems and human health.[1,2] Thus, a method for the comprehensive evaluation of multiple toxic metal ions in a polluted environment is urgently needed. To date, different methods, including inductively coupled plasma mass spectrometry (ICPMS),[3,4] atomic emission spectrometry (AES),[5,6] atomic absorption spectroscopy (AAS),[7,8] fluorescence spectroscopy,[9,10] and chromatography,[11,12] have been widely used for the detection of metal ions. However, these methods are associated with complex operation and sample preparation methods, which can only be performed under laboratory conditions. In particular, it is difficult to integrate these techniques with portable devices for on-site detection, especially for the simultaneous detection of multiple metal ions. However, this is exactly what is needed for environmental analysis.

Electrochemical analysis has shown great potential for on-site pollutant analysis. In particular, potentiometry combines the advantages of high sensitivity, portability, and easy integration for on-site detection.[13−16] Ion-selective electrodes (ISEs) are key components in potentiometry for allowing the selective identification of the target ions. In recent years, the development of all-solid-state ISEs has received considerable attention since such devices could provide long service lives, facile miniaturization, and nondestructive detection.[17,18] More importantly, compared to conventional ISEs, all-solid-state ISEs display significantly improved stability thanks to solid electronic conductors replacing the inner filling solution and the inner reference electrodes. All-solid-state ISEs have been used in portable,[19] online,[20,21] and wearable detection devices.[22,23] Paper-based screen-printed carbon electrodes (SPCEs), with unique advantages of flexible design, low cost, potential for mass production, and simple disposal, have received increasing interest for the fabrication of all-solid-state ISEs for potentiometric detection.[24−26] However, SPCEs are strongly influenced by the detection conditions, such as the influence from electrolyte background.[27] To date, no multichannel all-solid-state ISEs have been designed with an internal calibration system,[28−30] leading to limited accuracy in the ion detection. This is because the potential variations following the recognition of targets are generated not only by these events but also by the difference from the background. The introduction of an internal calibration system coupled with the potentiometric detection is highly desirable to improve the detection accuracy.

Herein, a novel all-solid-state potentiometric aptasensor array was developed to allow simultaneous detection of Hg^{2+}, Cd^{2+}, and As^{3+} with internal calibration based on open circuit potential (OCP) technology. This array was first modified with reduced graphene oxide (rGO) and gold with dendritic

Received: October 10, 2017
Accepted: June 25, 2018
Published: June 25, 2018

DOI: 10.1021/acs.analchem.7b04150
Anal. Chem. 2018, 90, 8337−8344

nanostructures (DenAu) to increase the stability and the effective area of SPCE channels, and then aptamers and the internal calibration DNA (IC-DNA)-labeled gold nanoparticles (AuNPs) were immobilized. In the presence of Hg^{2+}, Cd^{2+}, or As^{3+}, specific complexes were formed with the corresponding aptamers, resulting in a variation in the electrochemical potential. In order to avoid background influence from the detection system, a DNA sequence, composed of base A, was used to provide an internal calibration potential (ICP). This aptasensor array provided high sensitivity for the simultaneous detection of the three ions and was applied in real samples, indicating the great potential for the development of portable paper-based devices for the high-throughput analysis of environmental and clinical samples.

EXPERIMENTAL SECTION

Reagents and Materials. The following reagents and materials were used: tetrachloroaurate(III) tetrahydrate ($HAuCl_4{\cdot}4H_2O$, 47.8% Au) and graphite oxide (Nanjing Ji Cang Nano Tech Co., Ltd., Nanjing, China); 4,4′-biphenyldithiol (BPT) (Tokyo Chemical Industry Co., Ltd., Tokyo, Japan); $Cu(NO_3)_2$, $Hg(NO_3)_2$, $Ni(CH_3COO)_2$, $ZrCl_4$, $Fe(NO_3)_3$, $BaCl_2$, $ZnCl_2$, $CrCl_2$, KNO_3, $MnSO_4$, $Al_2(SO_4)_3$, $MgCl_2$, and $Pb(NO_3)_2$ (Sinopharm Chemical Reagent Co., Ltd., Shanghai, China); Cd(II) standard solution (1 mg mL^{-1}) and As(III) stock solution (1 mg mL^{-1}) (Merck Serono Co., Ltd., Shanghai, China); polypropylene (PP) synthetic paper (5 mm in thickness) (Shengcai Packaging Products Co., Ltd., Shanghai, China); insulating ink (Jelcon AC-3G, Jujo Chemical Company Co., Ltd., Japan); and DNA sequences (Shanghai Sangon Biological Engineering Technology & Service Co. Ltd., Shanghai, China) (Table S-1, S1.1, Supporting Information). The tap water, lake water, and river water samples were collected from our lab, the lake of Binjiang Park (Shanghai, China), and Huangpu River (Shanghai, China), respectively. All other chemicals were of analytical grade and were used without further purification. Ultrapure water (≥18 MΩ·cm), generated by a Millipore water purification system, was used throughout the experiments.

Apparatus and Measurements. The SPCE were made on an AT-25P instrument (Atma Champ Ent. Corp., China). Electrochemical impedance spectroscopy (EIS) and open circuit potential (OCP) measurements were carried out with a CHI660C electrochemical workstation (CH Instruments, Shanghai, China). The EIS measurements were performed with a conventional three-electrode system consisting of a modified SPCE working electrode, a Ag/AgCl reference electrode, and a platinum wire auxiliary electrode. OCP detection was conducted with a two-electrode system comprised of the modified SPCE (as an indicating electrode) and a Ag/AgCl reference electrode (filled with 3.0 M KCl). Morphologies of the modified electrode surfaces were characterized with scanning electron microscopy (SEM, Hitachi S-4800, Tokyo, Japan). The solid-state UV spectra were collected using a UV/vis/NIR spectrophotometer (Lambda 950, PerkinElmer, USA). The determination of real samples was verified by ICPMS (Element 2, Thermo Finnigan, Germany).

Fabrication of DenAu-Modified SPCE Channels. An SPCE with four channels was designed and prepared as reported before.[31,32] PP synthetic paper (5 mm in thickness) and a stencil were placed on the printing plates from the bottom up. Then, silver ink was printed and vacuum-dried for 20 min at 100 °C,[33] and this was followed by the successive printing of carbon layers for the fabrication of the working electrodes (Figure 1A), the connection port, and the insulating

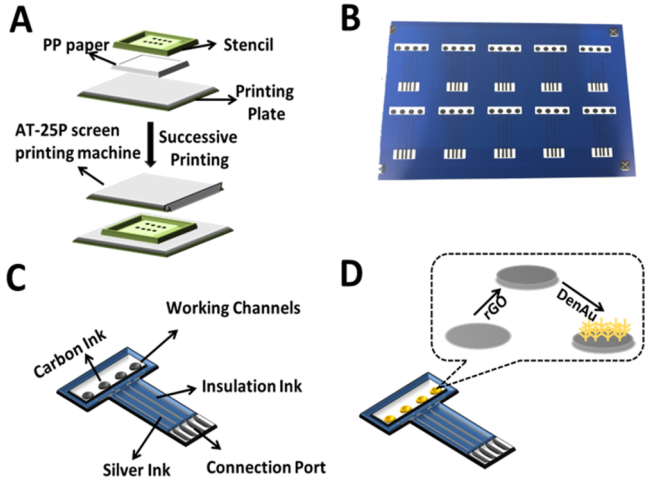

Figure 1. (A) Fabrication processes of the SPCE channels on PP synthetic paper. (B) Photograph of the multichannel SPCE sheet. (C) Structure of the multichannel SPCE. (D) Modification of rGO and DenAu on the SPCE channels.

layer to define the working electrode area with the same procedures. Thus, the final multichannel SPCE sheet containing 10 groups (Figure 1B) was obtained with the working area of each channel fixed at 0.07 cm^2 (3 mm in diameter). Figure 1C shows the structure of the SPCE channels. Graphene oxide was then electrochemically reduced in the SPCE channels in a N_2-purged dispersion (0.5 mg mL^{-1}) with magnetic stirring at a working potential of −0.8 V (vs Ag/AgCl) for 600 s.[24,34]

Afterward, DenAu were electrodeposited on the rGO-modified SPCE channels at −1.5 V in a mixture of 2.8 mM $HAuCl_4$ and 0.1 M H_2SO_4 (without stirring or N_2 bubbling) for 600 s,[35] to obtain the DenAu-modified SPCE (DenAu/rGO/SPCE) channels (Figure 1D).

Preparation of AuNPs-aptamer Probes and AuNPs-IC-DNA. AuNPs were prepared by a trisodium citrate reduction method as reported before.[36] Aqueous $HAuCl_4$ (100 mL, 1 mM) in a round-bottom flask was brought to boil with vigorous stirring. Then, 10 mL of 38.8 mM trisodium citrate was rapidly added to the boiling solution of $HAuCl_4$, and approximately 70 s later, the boiling mixture appeared red-violet in color. The resulting solution was stored at 4 °C in dark glass bottles for further use.

The synthesized AuNPs were further reacted with three thiolated aptamers (Table S-1, S1.1, Supporting Information), specific to Hg^{2+}, Cd^{2+}, and As^{3+}, and thiolated IC-DNA for 12 h at 37 °C in a 1:2 ratio (AuNPs:DNA sequences, v/v). Thus, the AuNPs-aptamer probes and AuNPs-IC-DNA were obtained, and the samples were stored at 4 °C until use (Scheme 1A).

Fabrication of the Aptasensor Array. The DenAu/rGO/SPCE was first activated by incubation in a 500 μM BPT/anhydrous ethanol solution for 6 h at room temperature. After that, the modified electrodes were washed twice with ethanol and distilled water sequentially. Then, 10 μL of the three AuNPs-aptamer probes and AuNPs-IC-DNA were self-assembled on the working area of the SPCE channels via BPT

DOI: 10.1021/acs.analchem.7b04150
Anal. Chem. 2018, 90, 8337−8344

Scheme 1. Schematic Illustration of (A) the Preparation of AuNPs-Aptamer Probes and AuNPs-IC-DNA and (B) the Fabrication of the Aptasensor Array and the Simultaneous Potentiometric Detection of Hg^{2+}, Cd^{2+}, and As^{3+}: a) the Immobilization of BPT, b) the Fabrication of the Aptasensor Array, c) the Recognition of Target Ions, and d) OCP Detection

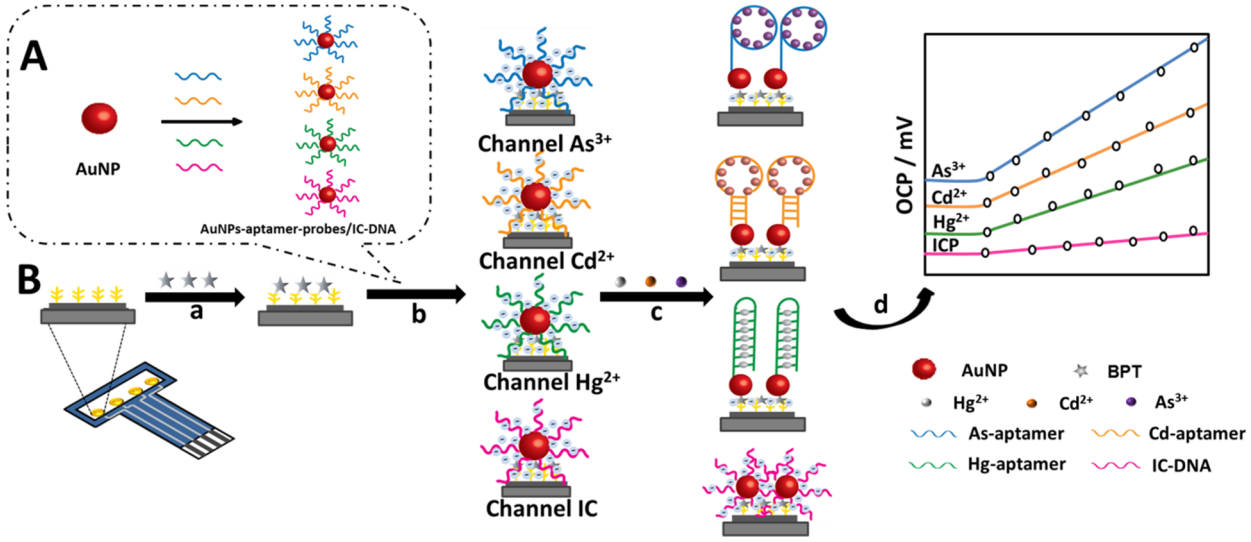

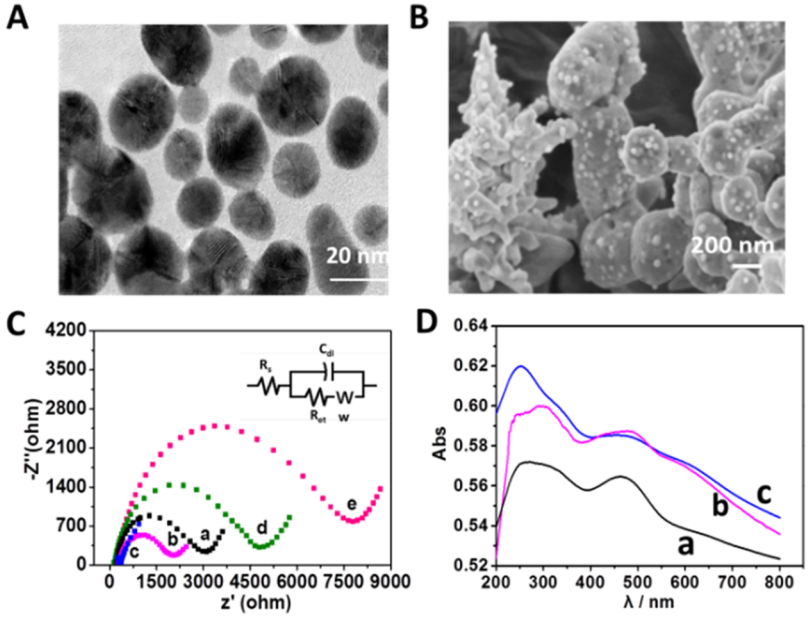

Figure 2. (A) TEM image of AuNPs. (B) SEM image of AuNPs-aptamers on the DenAu/rGO/SPCE channels. (C) EIS corresponding to each modification step of the SPCE channels in 5.0 mM $[Fe(CN)_6]^{4-}/[Fe(CN)_6]^{3-}$ solution containing 0.1 M KCl: (a) bare SPCE channels, (b) rGO/SPCE channels, (c) DenAu/rGO/SPCE channels, (d) BPT-modified DenAu/rGO/SPCE channels, and (e) AuNPs-aptamers-modified DenAu/rGO/SPCE channels. (D) Solid-state UV–vis spectra of (a) DenAu, (b) BPT/DenAu, and (c) AuNPs-aptamers-modified DenAu.

for 12 h at 37 °C (Scheme 1B), and then the samples were washed twice with 0.1 M PBS (pH = 7.4). The fabricated array was stored at 4 °C in a dry environment until use.[37,38]

Simultaneous Potentiometric Detection of Hg^{2+}, Cd^{2+}, and As^{3+}. To simultaneously detect Hg^{2+}, Cd^{2+}, and As^{3+}, the aptasensor array was incubated with 4 mL of a mixture of Hg^{2+}, Cd^{2+}, and As^{3+} at different concentrations in 0.1 M PBS (pH = 7.4) for 45 min at room temperature and then washed with 0.1 M PBS (pH = 7.4). Afterward, the OCP detection was performed in 0.1 M PBS (pH = 7.0) at room temperature. To evaluate the influence of nonspecific adsorption, the response of each aptasensor was recorded for 200 s until the equilibrium was reached. The ΔOCP values of the aptasensors were calculated according to the following equation: $\Delta OCP = OCP_n - OCP_a$, where OCP_a and OCP_n represent the potential of AuNPs-IC-DNA modified channel (Channel IC) as the ICP and potentials of Channel Hg^{2+}, Channel Cd^{2+}, and Channel As^{3+}, respectively.

RESULTS AND DISCUSSION

Characterization of the Aptasensor. To confirm the successful fabrication of the aptasensors, TEM, SEM, EIS, and UV–vis spectroscopy were employed. TEM image of the AuNPs indicates a homogeneous particles distribution with an average diameter of ~20 nm (Figure 2A). After the immobilization of the aptamers on the AuNPs, their size

DOI: 10.1021/acs.analchem.7b04150
Anal. Chem. 2018, 90, 8337–8344

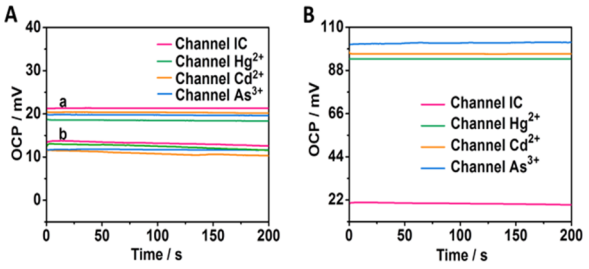

Figure 3. (A) OCP responses before (b) and after (a) immersion in 0.1 M PBS (pH = 7.4) without target ions for 45 min. (B) OCP responses of the aptasensor array after incubation with 2.5 μM Hg^{2+}, Cd^{2+}, and As^{3+} mixed solution for 45 min.

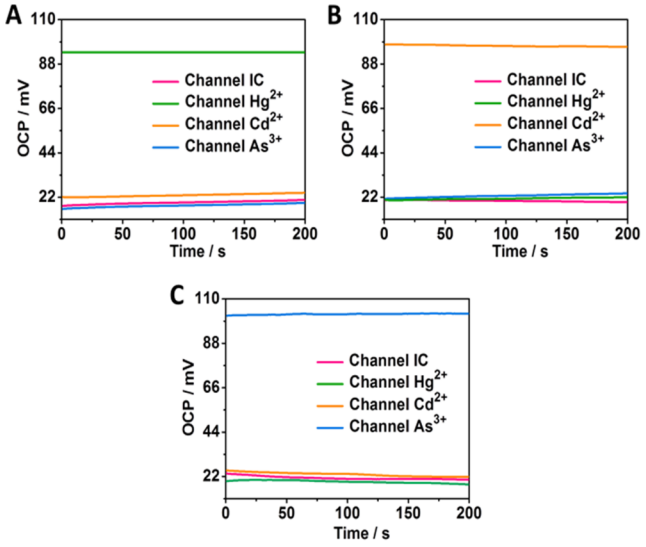

Figure 4. OCP responses of Channel IC, Channel Hg^{2+}, Channel Cd^{2+}, and Channel As^{3+} after respective incubation with (A) 2.5 μM Hg^{2+}, (B) 2.5 μM Cd^{2+}, or (C) 2.5 μM As^{3+}.

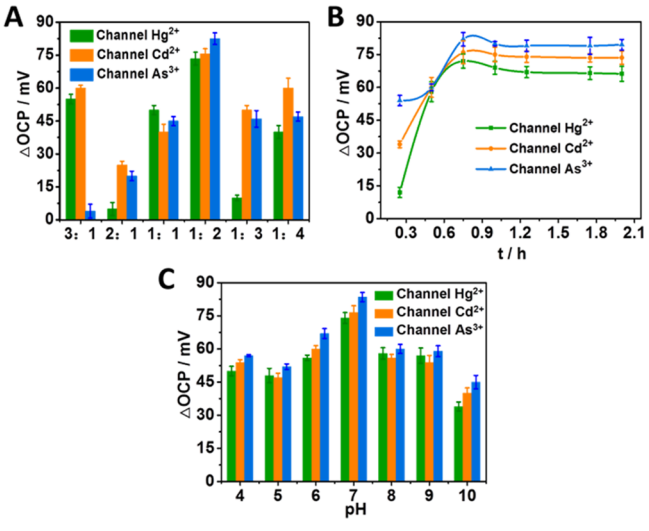

Figure 5. Effect of (A) the volume ratio of the AuNPs and DNA sequence (1.0 μM), (B) interaction time between the potentiometric aptasensor array and target ions, and (C) pH of the detection solution on the OCP responses of the aptasensor array. All the determinations were performed with a 2.5 μM Hg^{2+}, Cd^{2+}, and As^{3+} mixed solution. The error bars representing the standard deviation were derived from five electrodes.

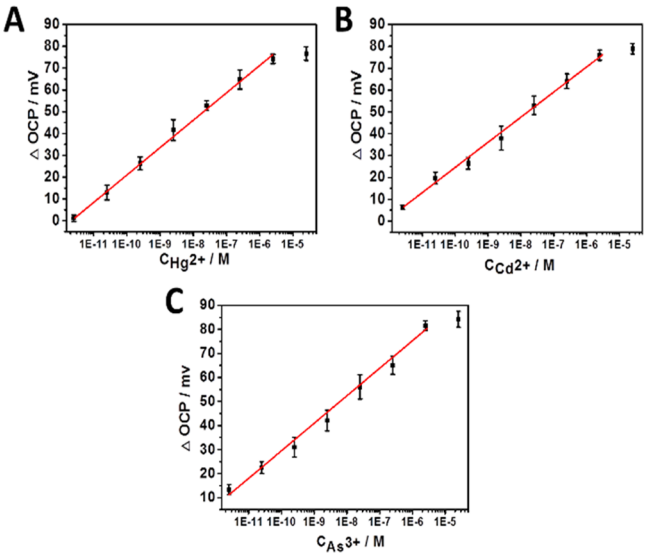

Figure 6. Linear curves of the ΔOCP obtained from Channel Hg^{2+} (A), Channel Cd^{2+} (B), and Channel As^{3+} (C) calibrated with Channel IC versus the logarithm of the Hg^{2+}, Cd^{2+}, and As^{3+} mixed solutions concentrations (2.5 pM, 25 pM, 0.25 nM, 2.5 nM, 25 nM, 0.25 μM, and 2.5 μM). The error bars representing the standard deviations were derived from five electrodes.

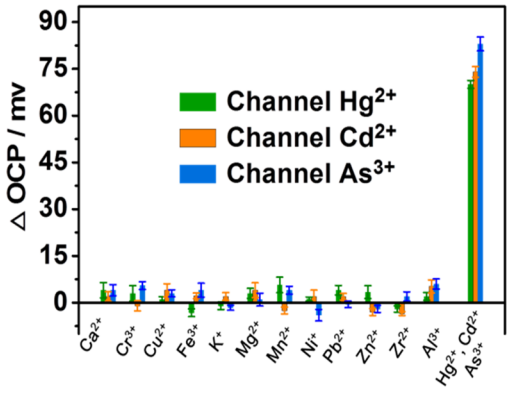

Figure 7. Selectivity of the potentiometric aptasensor array against 25 μM interfering ions added to a 2.5 μM Hg^{2+}, Cd^{2+}, and As^{3+} mixed solution. The error bars representing the standard deviations were derived from five electrodes.

increased to approximately 50 nm, as clearly visible in the SEM image of the AuNPs-aptamer probes on the DenAu/rGO/SPCE channels (Figure 2B). It could be observed that the electrodeposited DenAu with a special three-dimensional dendritic nanostructure has a large surface area, immobilizing numerous AuNPs-aptamer probes on its surface. In addition, the DenAu can control the orientation and density of the immobilized AuNPs-aptamer probes for the optimal recognition efficiency with target ions.[35] Therefore, the electrodeposited DenAu could improve the sensitivity of determination. Additionally, the SPCE, rGO/SPCE, and DenAu/rGO/SPCE channels were characterized by SEM (Figure S-1, S2.1, Supporting Information).

Figure 2C shows the variations of the EIS signal collected in the aptasensor array fabrication processes. The data were obtained by performing one of the SPCE channels in a 5.0 mM $[Fe(CN)_6]^{4-}/[Fe(CN)_6]^{3-}$ solution containing 0.1 M KCl with the frequency range from 10^5 to 0.1 Hz. Moreover, a

DOI: 10.1021/acs.analchem.7b04150
Anal. Chem. 2018, 90, 8337−8344

Table 1. Detection of Hg^{2+}, Cd^{2+}, and As^{3+} in Water Samples with the Proposed Method and ICPMS[a]

water samples	added (nM)	found (nM)			proposed method recovery (%, n = 5)			RSD (%)			found (nM)			ICPMS recovery (%, n = 5)			RSD (%)		
		Hg^{2+}	Cd^{2+}	As^{3+}	Hg^{2+}	Cd^{2+}	As^{3+}	Hg^{2+}	Cd^{2+}	As^{3+}	Hg^{2+}	Cd^{2+}	As^{3+}	Hg^{2+}	Cd^{2+}	As^{3+}	Hg^{2+}	Cd^{2+}	As^{3+}
tap water	0.00										0.06						2.43		
	5.00	4.83	5.05	4.98	96.61	101.01	99.63	3.32	4.92	2.01	4.82	4.68	4.93	96.41	93.62	98.62	4.03	3.13	2.54
	10.00	10.05	9.98	9.95	100.52	99.81	99.52	2.27	4.08	1.48	10.12	10.16	10.56	101.20	101.61	105.61	2.27	4.15	3.21
lake water	0.00																		
	5.00	5.03	4.97	5.11	100.61	99.43	102.21	3.05	3.42	2.35	5.08	5.27	5.01	101.63	105.40	100.20	3.05	4.08	1.21
	10.00	9.97	10.04	10.09	99.72	100.42	100.92	3.75	3.68	3.11	9.51	9.87	10.14	95.13	98.72	101.43	2.24	2.75	4.12
river water	0.00										0.02						1.05		
	5.00	4.96	5.03	4.95	99.21	100.61	99.01	2.78	3.97	4.41	4.96	5.03	5.11	99.21	100.61	102.22	2.56	2.02	2.42
	10.00	10.12	9.89	10.01	101.23	98.92	100.11	3.45	3.17	3.71	10.52	9.65	10.02	105.22	96.53	100.21	3.27	4.72	3.05

[a] n = 5.

Randles equivalent circuit diagram is shown (inset of Figure 2C), and it consists of the solution resistance (R_s), the charge transfer resistance between the electrode and the solution interface (R_{et}), the lipid bilayer capacitance (C_{dl}), and the Warburg impedance (W).[39,40] As previously reported, the semicircle diameter of the Nyquist curve was used to determine R_{et}.[41] Clearly, the bare SPCE channel shows a relatively high resistance (curve a, $R_{et} \approx 3098\ \Omega$). After the modification of the rGO membrane, the modified SPCE channel had a lower R_{et} value (curve b, $R_{et} \approx 2024\ \Omega$) due to the high conductivity and large surface area of the rGO membrane facilitating fast electron transfer to the SPCE channel surface. The subsequent modification by DenAu drastically decreased the R_{et} value (curve c, $R_{et} \approx 351\ \Omega$) due to both the extended surface area and excellent conductivity of DenAu. However, following the BPT self-assembly on the DenAu/rGO/SPCE channel, R_{et} obviously increased (curve d, $R_{et} \approx 4787\ \Omega$) because the thiol groups of BPT could block electron transfer at the interface. The further modification of AuNPs-aptamer probes induced a significant increase in the R_{et} value (curve e, $R_{et} \approx 7668\ \Omega$), which is mainly attributed to the successful fabrication of the aptasensor array with a weak conductivity, inhibiting the electron transfer due to the presence of the negatively charged phosphate backbone of the aptamers.[42]

The UV−vis spectra confirmed that the AuNPs-aptamer probes were bound to the DenAu immobilized on the substrate through BPT (Figure 2D). To eliminate the interference of rGO, the spectrum of a rGO-modified glass substrate was used as a blank baseline. The spectrum of DenAu shows a characteristic plasmon absorption peak at 505 nm (curve a), indicating its dense coverage on the substrate surface. The spectrum of BPT/DenAu exhibits characteristic plasmon absorption peaks representing BPT and DenAu, at 310 and 505 nm, respectively (curve b).[43,44] However, the intensity of the peak at 505 nm was weaker than that observed in curve a probably due to the occupied binding sites on the DenAu by BPT. After the AuNPs-aptamer probes were bound to BPT/DenAu, the intensity of the peak at 260 nm (curve c) obviously increased, indicating the formation of bioconjugates between BPT and AuNPs-aptamer probes and successful AuNPs-aptamer probes immobilization.[45]

Internal Calibration. In the potentiometric detection, the basic potential of the electrode may vary depending on the background, and it is thus independent from the target ions. If this effect is not taken into account using a calibration system, it would overlap with the potential change caused by target ions, leading to an inaccurate measurement. To improve the accuracy of the potentiometric measurement and decrease the background influence from the detection system, an internal calibration DNA (IC-DNA) sequence was needed. All-A sequence consisting of 100 A bases was employed as IC-DNA to provide an internal calibration potential. It is well-known that DNA chains display a large number of negatively charged phosphate groups,[27] thus the initial potential of the channels might be determined by the quantity of bases in the sequence, regardless of the actual identity of the nucleic acid. To verify this deduction, the potential of all-T sequence containing 100 T bases was recorded and compared with that of all-A sequence (Figure S-2, S2.2, Supporting Information), which revealed that these two sequences presented almost the same OCP responses. However, it has been reported that C, G, U, and T bases respectively present the preference for Ag^+, K^+,

DOI: 10.1021/acs.analchem.7b04150
Anal. Chem. 2018, 90, 8337−8344

and Hg^{2+},[46−48] probably leading to the generation of the inaccurate background potential. Therefore, all-A sequence was selected and designed with the same length as three specific aptamers (100 bases), providing a similar initial OCP response as those of the three aptasensors under the same conditions.

Figure 3A shows the OCP responses of the aptasensor array before and after being immersed in 0.1 M PBS (pH = 7.4) without target ions for 45 min. Immersion in PBS increased the signal intensity of all four channels due to the removal of the nonimmobilized AuNPs-aptamer probes and AuNPs-IC-DNA in the DenAu/rGO/SPCE channels, verifying that the variation of the background system influences indeed the OCP signals, and it is necessary to establish an internal calibration system. On the other hand, Channel IC with the immobilized IC-DNA in Figure 3A shows an OCP response similar to those of the three other channels even under different background conditions.

Following incubation in a 2.5 μM Hg^{2+}, Cd^{2+}, and As^{3+} mixed solution in 0.1 M PBS (pH = 7.4) for 45 min, the OCP values of Channel Hg^{2+}, Channel Cd^{2+}, and Channel As^{3+} increased dramatically (Figure 3B) due to the formation of specific rigid structures of the ions and the corresponding aptamers (Table S-1, S1.1, Supporting Information). Specifically, in the absence of target ions, the flexibility of the aptamer chains facilitated the flat arrangement of the aptamer chains on the surface of the DenAu/rGO SPCE channels, resulting in a high density of negative charges on the surface. With the addition of target ions, the aptamers would rather interact with target ions than remain attached to the surface. The formation of the rigid complexes caused the negative charge to move away from the surface. In other words, the negative charge density at the surface was reduced, increasing the OCP values.[49−52] In contrast, the Channel IC presented an almost constant response, which indicates that no IC-DNA interacted with the target ions to generate interference (Figure S-3, S2.2, Supporting Information). Thus, it is feasible to use IC-DNA to correct the background influence.

Evaluation of the Cross-Talk Behavior. To confirm that no electrochemical cross-talk occurred between neighboring channels, single target ion solutions with 2.5 μM of Hg^{2+}, Cd^{2+}, or As^{3+} were analyzed by the aptasensor array. As shown in Figure 4A, for the Hg^{2+} solution, only the potential of the Channel Hg^{2+} dramatically increased by 74 mV, while the potentials of the other channels did not vary. The same selectivity was observed for Channel Cd^{2+} (Figure 4B) and Channel As^{3+} (Figure 4C) with ΔOCP values varying from 76 to 82 mV, respectively (Figure S-4, S2.3, Supporting Information). The results show negligible interference between the three channels, indicating that the developed potentiometric aptasensor array can be used for simultaneous detection of Hg^{2+}, Cd^{2+}, and As^{3+}.

Optimization of the Experimental Conditions. To maximize the detection sensitivity, we optimized the following parameters: (1) ratio between the AuNPs and DNA sequences; (2) the interaction time between the potentiometric aptasensor array and the target ions; and (3) the pH value of the detection solution. Since the potential variation relies on both the labeled AuNPs-aptamer probes and the AuNPs-IC-DNA on the DenAu/rGO/SPCE channels, it is necessary to identify the volume ratio between the AuNPs and the DNA sequence to obtain a similar initial potential of the aptasensor array. As shown in Figure 5A, the ΔOCP values of the three channels reached their maximum at a volume ratio of 1:2 between the AuNPs and DNA sequences. As a result, 50 μL of synthetic AuNPs and 100 μL of 1.0 μM DNA sequences were added in 0.1 M PBS (pH = 7.4).

The amount of Hg^{2+}, Cd^{2+}, and As^{3+} captured by the aptasensor array could enhance the detection sensitivity. As seen in Figure 5B, the ΔOCP value increased when the interaction time was extended from 15 to 45 min, but beyond that, it remained almost the same due to the saturation of the recognition sites on the modified surface. Thus, 45 min was selected as the optimal interaction time, and it is comparable to that of other reported methods (Table S-2, S2.4, Supporting Information).

Figure 5C shows the variation in the ΔOCP values obtained in detection solutions at different pH's, which could affect the charge intensity and the activity of the complexes formed by the target ions and the aptamers. Obviously, the ΔOCP values increased as the pH increased from 4.0 to 7.0, while the ΔOCP values decreased as the pH further increased from 7.0 to 10.0. Therefore, a pH of 7.0 was selected as the optimal pH.

Simultaneous Detection of Hg^{2+}, Cd^{2+}, and As^{3+}. Under the optimal conditions, the potentiometric aptasensor arrays were incubated in Hg^{2+}, Cd^{2+}, and As^{3+} mixed solutions at different concentrations (2.5 pM, 25 pM, 0.25 nM, 2.5 nM, 25 nM, 0.25 μM, and 2.5 μM) in 0.1 M PBS (pH = 7.4) for 45 min, and then the OCP was determined in 0.1 M PBS (pH = 7.0). The calibration plots of the ΔOCP values for Hg^{2+}, Cd^{2+}, and As^{3+} were obtained using the potential of the Channel IC as the background signal (Figure 6). A good linear relationship was found between the ΔOCP values and the logarithm of the target ion concentrations in the range from 2.5 pM to 2.5 μM. At a higher concentration of target ions (25 μM), the increase in the ΔOCP values of the three channels became less pronounced probably due to the saturation of the available binding sites on the SPCE channel surface.[51,52] The corresponding equations are as follows: $\Delta OCP = 12.48\ lgC_{Hg}^{2+} + 146.42$ ($R = 0.9965$), $\Delta OCP = 11.56\ lgC_{Cd}^{2+} + 139.97$ ($R = 0.9979$), and $\Delta OCP = 11.24\ lgC_{As}^{3+} + 141.12$ ($R = 0.9951$). The detection limits were calculated as 2.0 pM (Figure 6A), 0.62 pM (Figure 6B), and 0.17 pM (Figure 6C) for Hg^{2+}, Cd^{2+}, and As^{3+} (S/N = 3), respectively. As mentioned before, the potential variation is caused by the rearrangement of the electrical charges on the surface of the DenAu/rGO/SPCE channels during the recognition event. Therefore, the potentiometric measurements do not follow the Nernstian response.[53,54]

Selectivity, Stability, and Reproducibility. The selectivity of the potentiometric aptasensor array was evaluated by testing other interfering ions, including 25 μM Ca^{2+}, Cr^{2+}, Cu^{2+}, Fe^{3+}, K^{+}, Mg^{2+}, Mn^{2+}, Ni^{2+}, Zn^{2+}, Zr^{2+}, Al^{3+}, and Cd^{2+} in the 2.5 μM Hg^{2+}, Cd^{2+}, and As^{3+} solution. As shown in Figure 7, the aptasensor array showed very little response to the interfering ions even when the concentration of the interfering ions was 10 times higher than that of target ions. The results indicate that the aptasensor array displays sufficient selectivity for the detection of Hg^{2+}, Cd^{2+}, and As^{3+}.

Moreover, the stability and reproducibility of the potentiometric aptasensor array were investigated in a 2.5 nM Hg^{2+}, Cd^{2+}, and As^{3+} solution. To assess the stability, five independent measurements were performed in 1 day with the same aptasensor array. The relative standard deviations (RSDs) obtained in the detection of Hg^{2+}, Cd^{2+}, and As^{3+} were 2.7%, 2.4%, and 2.4%, respectively, confirming the stability of the aptasensor array (Table S-3, S2.5, Supporting

DOI: 10.1021/acs.analchem.7b04150
Anal. Chem. 2018, 90, 8337−8344

Information). To evaluate the reproducibility, five aptasensor arrays were compared for the analysis of the same sample. The corresponding RSDs values for Hg^{2+}, Cd^{2+}, and As^{3+} were 3.3%, 4.0%, and 2.6%, respectively, showing an excellent reproducibility (Table S-4, S2.5, Supporting Information).

Detection of Hg^{2+}, Cd^{2+}, and As^{3+} in Real Samples. The applicability of the potentiometric aptasensor arrays was investigated in tap water, lake water, and river water (S2.6, Supporting Information). The real samples contain extremely low concentrations of Hg^{2+}, Cd^{2+}, and As^{3+}, which are not detectable.[55] Three target ions at 0.00, 5.00, and 10.00 nM were spiked into the real water samples, respectively, in order to illustrate the accuracy and anti-interference performance of the developed apatasensor array. Table 1 indicates a recovery range from 96.61% to 101.23% for Hg^{2+}, 98.92% to 101.01% for Cd^{2+}, and 99.01% to 102.21% for As^{3+} with acceptable RSDs. Moreover, the results obtained with the proposed aptasensor array are in good agreement with the measurement by ICPMS. Thus, these results confirmed that the aptasensor array can be applied to the analysis of real samples with both high accuracy and precision.

CONCLUSIONS

In this study, we demonstrated a novel all-solid-state potentiometric aptasensor array for the simultaneous detection of Hg^{2+}, Cd^{2+}, and As^{3+} based on a multichannel SPCE combining rGO and DenAu modifications. Owing to the specific recognition of the target ions by the corresponding aptamer-labeled AuNPs, the ions could be captured by the aptasensor array and determined with an OCP technique. IC-DNA was used to provide the internal calibration potential, allowing the background influence to be subtracted. Under the optimized conditions, the ΔOCP values present good linear correlations with the logarithm of the Hg^{2+}, Cd^{2+}, and As^{3+} concentrations in the range of 2.5 pM to 2.5 μM with detection limits of 2.0 pM, 0.62 pM, and 0.17 pM, respectively. Moreover, it has been verified that there is no mutual interference between the target ions or with other ions, reflecting the excellent selectivity of this developed device. The aptasensor array was further applied to analyze Hg^{2+}, Cd^{2+}, and As^{3+} in real samples, and the results were validated by the data obtained with ICPMS measurements. The satisfactory accuracy and precision indicate the great potential of aptasensor arrays in the development of portable devices for the on-site detection of multiple heavy metal ions.

ASSOCIATED CONTENT

Supporting Information

The Supporting Information is available free of charge on the ACS Publications website at DOI: 10.1021/acs.analchem.7b04150.

Additional information as noted in text; list of DNA sequences; SEM images of the modified SPCE channels; stability of the potentiometric aptasensor array; reproducibility study of the potentiometric aptasensor array (PDF)

AUTHOR INFORMATION

Corresponding Author

*Phone/Fax: +86-21-54340049. E-mail: fzhang@chem.ecnu.edu.cn.

ORCID

Fan Zhang: 0000-0003-4229-3916

Notes

The authors declare no competing financial interest.

ACKNOWLEDGMENTS

This work was financially supported by the National Natural Science Foundation of China (Grant Nos. 21575042 and 21405049).

REFERENCES

(1) Zahir, F.; Rizwi, S. J.; Haq, S. K.; Khan, R. H. *Environ. Toxicol. Pharmacol.* **2005**, *20*, 351−360.
(2) Selin, N. E. *Annu. Rev. Environ. Resour.* **2009**, *34*, 43.
(3) Chen, X.; Han, C.; Cheng, H.; Wang, Y.; Liu, J.; Xu, Z.; Hu, L. J. *Chromatogr., A* **2013**, *1314*, 86−93.
(4) Townsend, A. T.; O'Sullivan, J.; Featherstone, A. M.; Butler, E. C. V.; Mackey, D. J. *J. Environ. Monit.* **2001**, *3*, 113−120.
(5) Matusiewicz, H.; Horvath, Z.; Barnes, R. M. *Appl. Spectrosc.* **1985**, *39*, 558−560.
(6) Webb, M. R.; Andrade, F. J.; Hieftje, G. M. *Anal. Chem.* **2007**, *79*, 7807−7812.
(7) West, C. D. *Anal. Chem.* **1974**, *46*, 797−803.
(8) Winefordner, J. D.; Elser, R. C. *Anal. Chem.* **1971**, *43*, 24−29.
(9) Winefordner, J. D.; Staab, R. A. *Anal. Chem.* **1964**, *36*, 1367−1369.
(10) Howes, P. D.; Chandrawati, R.; Stevens, M. M. *Science* **2014**, *346*, 53−64.
(11) Sarzanini, C.; Bruzzoniti, M. C. *TrAC, Trends Anal. Chem.* **2001**, *20*, 304−310.
(12) Bin Abas, M. R.; Takruni, I. A.; Abdullah, Z.; Tahir, N. M. *Talanta* **2002**, *58*, 883−890.
(13) Liang, R. N.; Ding, J. W.; Gao, S. S.; Qin, W. *Angew. Chem., Int. Ed.* **2017**, *56*, 6833−6837.
(14) Cuartero, M.; Pankratova, N.; Cherubini, T.; Crespo, G. A.; Massa, F.; Confalonieri, F.; Bakker, E. *Environ. Sci. Technol. Lett.* **2017**, *4*, 410−415.
(15) Tarasov, A.; Gray, D. W.; Tsai, M. Y.; Shields, N.; Montrose, A.; Creedon, N.; Lovera, P.; O'Riordan, A.; Mooney, M. H.; Vogel, E. M. *Biosens. Bioelectron.* **2016**, *79*, 669−678.
(16) Pankratova, N.; Cuartero, M.; Cherubini, T.; Crespo, G. A.; Bakker, E. *Anal. Chem.* **2017**, *89*, 571−575.
(17) Bakker, E.; Pretsch, E.; Bühlmann, P. *Anal. Chem.* **2000**, *72*, 1127−1133.
(18) Bakker, E.; Pretsch, E. *Angew. Chem., Int. Ed.* **2007**, *46*, 5660−5668.
(19) Hu, J. B.; Ho, K. T.; Zou, X. U.; Smyrl, W. H.; Stein, A.; Bühlmann, P. *Anal. Chem.* **2015**, *87*, 2981−2987.
(20) Abd El-Rahman, M. K.; Zaazaa, H. E.; ElDin, N. B.; Moustafa, A. A. *Talanta* **2015**, *132*, 52−58.
(21) Ding, J. W.; Li, B. W.; Chen, L. X.; Qin, W. *Angew. Chem., Int. Ed.* **2016**, *55*, 13033−13037.
(22) Gao, W.; Emaminejad, S.; Nyein, H. Y. Y.; Challa, S.; Chen, K.; Peck, A.; Fahad, H. M.; Ota, H.; Shiraki, H.; Kiriya, D.; Lien, D.-H.; Brooks, G. A.; Davis, R. W.; Javey, A. *Nature* **2016**, *529*, 509−514.
(23) Nyein, H. Y. Y.; Gao, W.; Shahpar, Z. B.; Emaminejad, S.; Challa, S.; Chen, K.; Fahad, H. M.; Tai, L. C.; Ota, H.; Davis, R. W.; Javey, A. *ACS Nano* **2016**, *10*, 7216−7224.
(24) Ping, J. F.; Wang, Y. X.; Ying, Y. B.; Wu, J. *Anal. Chem.* **2012**, *84*, 3473−3479.
(25) Cui, J.; Lisak, G.; Strzalkowska, S.; Bobacka, J. *Analyst* **2014**, *139*, 2133−2136.
(26) Lan, W. J.; Zou, X. U.; Hu, J.; Parolo, C.; Maxwell, E. J.; Bühlmann, P.; Whitesides, G. M. *Anal. Chem.* **2014**, *86*, 9548−9553.
(27) Ding, J. W.; Gu, Y.; Li, F.; Zhang, H. X.; Qin, W. *Anal. Chem.* **2015**, *87*, 6465−6469.

DOI: 10.1021/acs.analchem.7b04150
Anal. Chem. 2018, 90, 8337−8344

(28) Lin, Y. H.; Wang, S. H.; Wu, M. H.; Pan, T. M.; Lai, C. S.; Luo, J. D.; Chiou, C. C. *Biosens. Bioelectron.* **2013**, *43*, 328−335.
(29) Toczyłowska-Mamińska, R.; Kloch, M.; Zawistowska-Deniziak, A.; Bala, A. *Talanta* **2016**, *159*, 7−13.
(30) Wang, S. Q.; Wu, Y. J.; Gu, Y.; Li, T.; Luo, H.; Li, L. H.; Bai, Y. Y.; Li, L. L.; Liu, L.; Gao, Y. D.; Ding, H. Y.; Zhang, T. *Anal. Chem.* **2017**, *89*, 10224−10231.
(31) Song, W.; Zhang, L.; Shi, L.; Li, D. W.; Li, Y.; Long, Y. T. *Microchim. Acta* **2010**, *169*, 321−326.
(32) Li, M.; Li, Y. T.; Li, D. W.; Long, Y. T. *Anal. Chim. Acta* **2012**, *734*, 31−44.
(33) Li, D.; Li, D. W.; Fossey, J. S.; Long, Y. T. *Anal. Chem.* **2010**, *82*, 9299−9305.
(34) Ping, J. F.; Wang, Y. X.; Fan, K.; Wu, J.; Ying, Y. B. *Biosens. Bioelectron.* **2011**, *28*, 204−209.
(35) Li, F.; Han, X. P.; Liu, S. F. *Biosens. Bioelectron.* **2011**, *26*, 2619−2625.
(36) Liang, X. S.; Wei, H. P.; Cui, H. P.; Deng, J. Y.; Zhang, Z. P.; You, X. Y.; Zhang, X. E. *Analyst* **2011**, *136*, 179−183.
(37) Yang, Y. C.; Li, C.; Yin, L.; Liu, M. Y.; Wang, Z. X.; Shu, Y. Q.; Li, G. X. *ACS Appl. Mater. Interfaces* **2014**, *6*, 7579−7584.
(38) Li, C.; Yang, Y. C.; Wei, L. M.; Wang, X. Y.; Wang, Z. X.; Ying, Y. M.; Li, G. X. *Theranostics* **2015**, *5*, 62−70.
(39) Qiu, Z. L.; Shu, J.; Jin, G. X.; Xu, M. D.; Wei, Q. H.; Chen, G. N.; Tang, D. P. *Biosens. Bioelectron.* **2016**, *77*, 681−686.
(40) Li, C. C.; Guo, X. Y.; Shen, S.; Song, P.; Xu, T.; Wen, Y.; Yang, H. F. *Corros. Sci.* **2014**, *83*, 147−154.
(41) Hou, L.; Gao, Z. Q.; Xu, M. D.; Cao, X.; Wu, X. P.; Chen, G. N.; Tang, D. P. *Biosens. Bioelectron.* **2014**, *54*, 365−371.
(42) Yan, M.; Zang, D. J.; Ge, S. G.; Ge, L.; Yu, J. H. *Biosens. Bioelectron.* **2012**, *38*, 355−361.
(43) Kalachyova, Y.; Mares, D.; Jerabek, V.; Zaruba, K.; Ulbrich, P.; Lapcak, L.; Svorcik, V.; Lyutakov, O. *J. Phys. Chem. C* **2016**, *120*, 10569−10577.
(44) Weckenmann, U.; Mittler, S.; Naumann, K.; Fischer, R. A. *Langmuir* **2002**, *18*, 5479−5486.
(45) Dong, H. F.; Meng, X. D.; Dai, W. H.; Cao, Y.; Lu, H. T.; Zhou, S. F.; Zhang, X. J. *Anal. Chem.* **2015**, *87*, 4334−4340.
(46) Guo, W. W.; Qi, X. J.; Orbach, R.; Lu, C. H.; Freage, L.; Mironi-Harpaz, I.; Seliktar, D.; Yang, H. H.; Willner, I. *Chem. Commun.* **2014**, *50*, 4065−4068.
(47) Li, T.; Wang, E.; Dong, S. J. *Anal. Chem.* **2010**, *82*, 7576−7580.
(48) Marino, T. *J. Mol. Model* **2014**, *20*, 2303.
(49) Zelada-Guillén, G. A.; Bhosale, S. V.; Riu, J.; Rius, F. X. *Anal. Chem.* **2010**, *82*, 9254−9260.
(50) Zelada-Guillén, G. A.; Sebastián-Ávila, J. L.; Blondeau, P.; Riu, J.; Rius, F. X. *Biosens. Bioelectron.* **2012**, *31*, 226−232.
(51) Zelada-Guillén, G. A.; Riu, J.; Düzgün, A.; Rius, F. X. *Angew. Chem., Int. Ed.* **2009**, *48*, 7334−7337.
(52) Hernández, R.; Vallés, C.; Benito, A. M.; Maser, W. K. *Biosens. Bioelectron.* **2014**, *54*, 553−557.
(53) Düzgün, A.; Zelada-Guillén, G. A.; Crespo, G. A.; Macho, S.; Riu, J.; Rius, F. X. *Anal. Bioanal. Chem.* **2011**, *399*, 171−181.
(54) Zhou, Y.; Yu, B.; Guiseppi-Elie, A.; Sergeyev, V.; Levon, K. *Biosens. Bioelectron.* **2009**, *24*, 3275−3280.
(55) Chen, G. H.; Chen, W. Y.; Yen, Y. C.; Wang, C. W.; Chang, H. T.; Chen, C. F. *Anal. Chem.* **2014**, *86*, 6843−6849.

DOI: 10.1021/acs.analchem.7b04150
Anal. Chem. 2018, 90, 8337−8344